Complete analysis of all $B \to \pi K$ decays

Anirban Kundu,[1,*] Sunando Kumar Patra,[2,†] and Shibasis Roy[1,‡]
[1]*Department of Physics, University of Calcutta, 92 Acharya Prafulla Chandra Road, Kolkata 700009, India*
[2]*Department of Physics, Bangabasi Evening College, 19 Rajkumar Chakraborty Sarani, Kolkata 700009, India*

(Received 5 July 2021; revised 23 September 2021; accepted 1 November 2021; published 30 November 2021)

The Standard Model (SM) predicts that ΔA_{CP}, the difference between the direct CP asymmetries for the modes $B^+ \to \pi^0 K^+$ and $B^0 \to \pi^- K^+$ that are related by a weak isospin, should be close to zero. There has been a recent claim by the LHCb Collaboration that the measured value of ΔA_{CP} shows an uncomfortable tension with the SM prediction, almost at the 8σ level. Motivated by this claim, we critically reexamine the data on all the $B \to \pi K$ modes, including the CP asymmetries and CP-averaged branching fractions. From a combined Bayesian analysis with the topological amplitudes and their phases as the free parameters, we find that the best-fit region has a large overlap with the parameter space favored in the SM, albeit with some enhancement for the electroweak penguin and the color-suppressed tree amplitudes; consistent with the findings of earlier studies. We find that in this SM-like region, ΔA_{CP} is more than 5σ away from zero and the tension with the global average, as well as the LHCb result, is within 2σ. Thus, we conclude that there is not yet enough motivation to go beyond the SM.

DOI: 10.1103/PhysRevD.104.095025

I. INTRODUCTION

The neutral and charged B-mesons decaying to a πK pair, namely, $B^+ \to \pi^0 K^+$, $\pi^+ K^0$, and $B^0 \to \pi^- K^+$, $\pi^0 K^0$ (plus the CP-conjugate channels), continue to show some tension when the four branching ratios (BR), four direct CP asymmetries and the mixing-induced CP asymmetry in $B^0 \to \pi^0 K^0$ are compared with the Standard Model (SM) predictions. This is, in essence, the "$B \to \pi K$ puzzle" [1–4]; the experimental data from the *BABAR* [5–9], Belle [10,11], LHCb [12–14], and very recently, Belle-II [15–17] Collaborations have continued to provide support for the puzzle. Recently, the LHCb Collaboration have updated the data on the difference of the direct CP asymmetries [18] between the modes $B^+ \to \pi^0 K^+$ and $B^0 \to \pi^- K^+$, defined as ΔA_{CP}

$$\Delta A_{CP}^{\mathrm{LHCb}}(\pi K) = 0.108 \pm 0.017 \tag{1}$$

that is nonzero with a significance of more than six standard deviations, while the global average

$$\Delta A_{CP}^{\mathrm{global}}(\pi K) = 0.115 \pm 0.014 \tag{2}$$

lies a remarkable eight standard deviations away from zero, which happens to be the SM prediction [19] for ΔA_{CP}. The null prediction of the SM is based on the relative importance of certain flavor-flow topologies [19] as well as on the assumption that the difference in strong phase between the tree and electroweak penguin amplitudes is identically zero. The goal of this paper is to check the robustness of these claims.

A good way of writing these topological amplitudes is shown in Ref. [20–22], which we follow. We first enlist all the relevant amplitudes [21], including the possible weak and strong phases. The details can be found in Sec. II A. We implicitly assume that the weak phase comes solely from the Cabibbo-Kobayashi-Maskawa (CKM) mixing matrix elements, while the strong phases can be arbitrary. The latter come mostly from long-distance rescattering effects [23–27], so one may theoretically expect some relationship among the strong phases [28–34] associated with various amplitudes (up to a certain level of precision), but we try to avoid such theoretical prejudices as much as possible. The analysis treats all the amplitudes and relevant strong phases as free parameters, while the CKM elements and weak phases are incorporated as multinormal priors. The numbers on any specific observable coming from different experiments are treated as independent inputs in the absence of any correlation, i.e., we do not take the average values for the observables. This, naturally, enhances the

*akphy@caluniv.ac.in
†sunando.patra@gmail.com
‡shibasis.cmi@gmail.com

number of data points. For the justification of this approach, and for the methodology of the analysis, we refer the reader to Sec. III.

What we find is not completely unexpected in view of the previous analyses [35–46], but sheds some interesting light on the so-called puzzle. The salient features, discussed in more detail in Sec. IV, are as follows:

(i) We performed a Bayesian analysis with uniform priors on the topological amplitudes and phases supplied over a wide range. We have also checked that this region contains the χ^2-minimum of the frequentist analysis.

(ii) With a naive estimate of the relative importance of the amplitudes [20,21,47], there is no acceptable fit to the data. This estimate is mostly based on the CKM factors present in each amplitude; the smallness is controlled by λ, the sine of the Cabibbo angle ($\sim$0.22). Another important parameter that comes into play is the ratio of the Wilson coefficients (WC) of the electroweak penguin and tree operators. There is no reason why the low-energy QCD corrections, including the effects coming from the running of the WCs of the relevant operators, should still respect these estimates. Thus, based on this part of the analysis, one must not say that the SM is ruled out.

(iii) One might like to relax the bounds on the color-suppressed tree amplitudes to cover possible nonperturbative QCD effects [28,29,33,48–54] as well as the electroweak penguin amplitudes.

This, in effect, should cover the entire SM-allowed region, but some of the amplitudes may be enhanced compared to the naive fit. As such enhancements are not ruled out even within the framework of the SM, this is what we call the 'SM-like' region, more details of which are given later. However, one may also invoke new physics (NP) to explain this [55–60]. In this SM-like parameter space with possibilities of NP playing a role [37–44,61] lies the best-fit region, with ΔA_{CP} more than 5σ away from zero, and with a tension of less than 2σ with the global average. This leads to our main conclusion; the data is still not at variance with the SM, and the discrepancy in ΔA_{CP} is not something to claim the existence of NP. However, presence of NP cannot be ruled out either.

(iv) Finally, we entertain the possibility of NP in $B \to \pi K$, which might affect the amplitudes, as well as the WCs. We perform a free fit, relaxing the SM limit on the amplitudes. In the SM, the ratio of the electroweak penguin amplitude to the tree amplitude is approximately the same, for both color-allowed and color-suppressed channels. In the free fit, these two ratios may also possibly differ. We find that there appears another best-fit region, but definitely beyond the SM-allowed parameter space.

One might ask whether there is any way to differentiate between these two best-fit regions and know for sure which is the actual one. We show that there are two possible ways. The SM-like prediction for ΔA_{CP} is about 2σ away from the global average; if the data becomes more precise and the tension increases, it might point to the presence of NP. Alternatively, a suitably defined combination of the branching ratios and CP asymmetries of these four channels may also have the potential to do the job.

The paper, thus, is arranged as follows. In Sec. II A, we display the relevant expressions, and lay out the relevant parameter spaces. Section III is about the analysis, while we show our results in Sec. IV. Section V summarizes and concludes the paper.

II. THEORY INPUTS

A. Topological amplitudes and phases

The four $B \to \pi K$ decay amplitudes can be parametrized in at least two different ways. The first one is by three isospin amplitudes [19,62–64] $A_{1/2}$, $A_{3/2}$, and $B_{1/2}$, where A and B respectively stand for $\Delta I = 1$ and $\Delta I = 0$ amplitudes, and the subscript denotes the isospin of the πK combination. In this notation, the amplitudes are written as [64]

$$\begin{aligned} A(B^+ \to \pi^+ K^0) &= B_{1/2} + A_{1/2} + A_{3/2}, \\ A(B^+ \to \pi^0 K^+) &= -\frac{1}{\sqrt{2}}(B_{1/2} + A_{1/2}) + \sqrt{2}A_{3/2}, \\ A(B^0 \to \pi^- K^+) &= -B_{1/2} + A_{1/2} + A_{3/2}, \\ A(B^0 \to \pi^0 K^0) &= \frac{1}{\sqrt{2}}(B_{1/2} - A_{1/2}) + \sqrt{2}A_{3/2}. \end{aligned} \tag{3}$$

The QCD penguin diagram contributes only to the isospin amplitude $B_{1/2}$ and hence it is the largest among the three. Each such amplitude is actually made of two parts, with two independent CKM factors. Thus, one has six independent amplitudes and therefore five independent strong phase differences.

The hierarchy among the amplitudes is even more evident if we consider the topological amplitudes [65–69]. There are four distinct topological classes, namely, "color-allowed tree" T, "color-suppressed tree" C, "annihilation" A, and "penguin". These topologies are shown in Fig. 1, taken from [20,21]. The penguin topology is further subdivided into strong penguin P, color-allowed electroweak penguin (EWP) $P_{\rm EW}$, and color-suppressed EWP $P^C_{\rm EW}$. Each amplitude carries its own strong phase, but only the phase differences are relevant, as an overall phase does not have any effect on the observables.

The decay amplitudes for $B^0 \to \pi^- K^+$, $B^+ \to \pi^+ K^0$, $B^0 \to \pi^0 K^0$, and $B^+ \to \pi^0 K^+$, from now on denoted by

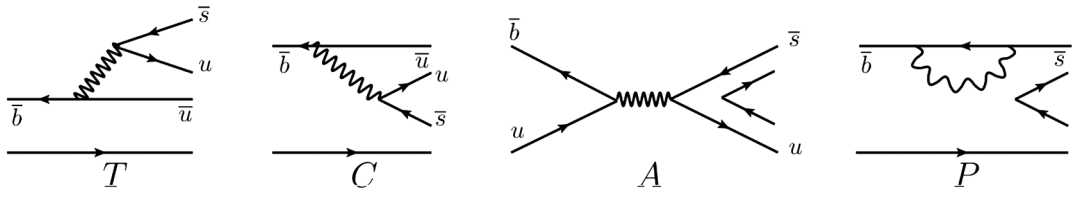

FIG. 1. Topological amplitudes for $B \to \pi K$ decays, taken from Ref. [20].

$\mathcal{A}^{-+}$, $\mathcal{A}^{+0}$, $\mathcal{A}^{00}$, $\mathcal{A}^{0+}$ respectively, may be expressed in terms of the topological amplitudes [20,21,70,71] as

$$\begin{aligned}
\mathcal{A}^{-+} &= -\lambda_u(P_{uc}+T) - \lambda_t\left(P_{tc}+\frac{2}{3}P_{\mathrm{EW}}^{C}\right),\\
\mathcal{A}^{+0} &= \lambda_u(P_{uc}+A) + \lambda_t\left(P_{tc}-\frac{1}{3}P_{\mathrm{EW}}^{C}\right),\\
\sqrt{2}\mathcal{A}^{00} &= \lambda_u(P_{uc}-C) + \lambda_t\left(P_{tc}-P_{\mathrm{EW}}-\frac{1}{3}P_{\mathrm{EW}}^{C}\right),\\
\sqrt{2}\mathcal{A}^{0+} &= -\lambda_u(P_{uc}+T+C+A) - \lambda_t\left(P_{tc}+P_{\mathrm{EW}}+\frac{2}{3}P_{\mathrm{EW}}^{C}\right),
\end{aligned} \tag{4}$$

where we have factored out the CKM elements $\lambda_q = V_{qb}^{*}V_{qs}$ from the amplitudes. We note that the penguin amplitude P receives contributions from all the three up-type quarks in the loop

$$P = \lambda_u P_u + \lambda_c P_c + \lambda_t P_t, \tag{5}$$

and the unitarity of the CKM matrix

$$\lambda_u + \lambda_c + \lambda_t = 0, \tag{6}$$

leads to

$$P = \lambda_u(P_u - P_c) + \lambda_t(P_t - P_c) \equiv \lambda_u P_{uc} + \lambda_t P_{tc}. \tag{7}$$

We expect a hierarchy among these amplitudes, which, magnitude wise, looks like

$$|\lambda_t P_{tc}| > |\lambda_u T| > |\lambda_u C| > |\lambda_u A|, \qquad |\lambda_u P_{uc}|, \tag{8}$$

where every subsequent step is suppressed compared to the previous one by a factor of the order of $\lambda \approx \sin\theta_C = 0.22$, θ_C being the Cabibbo angle. The suppression is a combined effect of the magnitudes of the respective CKM elements and the extra loop suppression of the penguin amplitudes. For example, $\lambda_u/\lambda_t \sim \lambda^2$, but P_{tc} is loop suppressed compared to T, again by an order of λ [22]. It also turns out that $|C/T| \sim \lambda$ [33]. However, even within the SM, $|C/T| \sim 0.5$ is definitely possible [52], which we will use in our analysis. One may note that this ratio of the order of unity [32,34] is also not ruled out. The annihilation amplitude A is suppressed by a factor of $f_B/m_B \sim 0.05 \sim \lambda^2$ when compared to T. The long-distance rescattering effects should modify these predictions, but if the color-transparency argument holds for $B \to \pi K$, we do not expect a drastic reordering. Thus, anything widely off from Eq. (8) signals the presence of NP. On the other hand, one must remain open to the possibility that the hierarchy may not be all that sacrosanct; an enhancement by $\mathcal{O}(1/\lambda) \sim 5$ for some cases even within the framework of SM may not be discarded offhand.

A relation between the tree and the EWP amplitudes may be obtained with the help of $SU(3)$-flavor symmetry of the dimension-six weak Hamiltonian mediating the $|\Delta S| = 1$ decay [72,73],

$$\begin{aligned}
\mathcal{H}(\Delta S = 1) = \frac{G_F}{\sqrt{2}}\Big[&\lambda_u\big(C_1(\bar{b}u)_{V-A}(\bar{u}s)_{V-A}\\
&+ C_2(\bar{b}s)_{V-A}(\bar{u}u)_{V-A}\big) - \lambda_t\sum_{i=3}^{10} C_i Q_i\Big],
\end{aligned} \tag{9}$$

where Q_{1-2} are the tree, Q_{3-6} are the QCD penguin and Q_9, Q_{10} are the two non-negligible EWP operators in the SM. The P_{EW} and P_{EW}^{C} amplitudes are therefore given in terms of T and C respectively [67,68,73],

$$P_{\mathrm{EW}} \pm P_{\mathrm{EW}}^{C} = -\frac{3}{2}\frac{C_9 \pm C_{10}}{C_1 \pm C_2}(T \pm C). \tag{10}$$

After plugging in the numerical values of the WCs C_1, C_2, C_9, and C_{10} to the leading-log order at m_b scale [72], one gets

$$P_{\mathrm{EW}} \sim \kappa T, \qquad P_{\mathrm{EW}}^{C} \sim \kappa C, \tag{11}$$

to a good approximation, where

$$\kappa = -\frac{3}{2}\frac{C_9 + C_{10}}{C_1 + C_2} \simeq -\frac{3}{2}\frac{C_9 - C_{10}}{C_1 - C_2} \simeq 0.0135 \pm 0.0012. \tag{12}$$

One may note that in the SM, both P_{EW}/T and P_{EW}^{C}/C are approximately the same. This need not be true in the presence of NP, or even some yet to be accounted for SM dynamics. As the κ-suppression compensates the λ_t/λ_u enhancement, one may infer that $|\lambda_t P_{\mathrm{EW}}| \sim |\lambda_u T|$ and $|\lambda_t P_{\mathrm{EW}}^{C}| \sim |\lambda_u C|$. Thus, these two amplitudes may have a

non-negligible contribution to branching fractions and CP asymmetries for $B \to \pi K$ decays.

It is worth mentioning here that any NP contributing to $P_{\rm EW}$ simultaneously affects C as well, as their respective contributions enter the decay amplitudes in Eq. (4) exclusively in a particular combination [56]. This attribute is not limited to the above mentioned combination of diagrammatic amplitudes, but is an artifact of redundancy in the definition of them. This is known as reparametrization invariance, and prevents a clean extraction of NP affecting a particular amplitude from the available experimental observations.

B. CP asymmetries

The decay rate asymmetry for any $B \to \pi K$ process is defined as

$$\Delta(\pi K) = \Gamma(b) - \Gamma(\bar{b}), \tag{13}$$

where $\Gamma(b)$ and $\Gamma(\bar{b})$ are the decay rates of the CP-conjugate mesons containing a b-quark (i.e., B^- or $\overline{B^0}$) or a $\bar{b}$ quark (i.e., B^+ or B^0) respectively. In terms of the topological amplitudes, the four $B \to \pi K$ decay rate asymmetries [71] are given by

$$\begin{aligned}
\Delta(\pi^- K^+) &= -4\mathrm{Im}(\lambda_u^* \lambda_t)\mathrm{Im}\left[(T + P_{uc})^* \left(P_{tc} + \frac{2}{3}P_{\rm EW}^C\right)\right], \\
2\Delta(\pi^0 K^+) &= -4\mathrm{Im}(\lambda_u^* \lambda_t)\mathrm{Im}\left[(T + C + A + P_{uc})^* \left(P_{tc} + P_{\rm EW} + \frac{2}{3}P_{\rm EW}^C\right)\right], \\
2\Delta(\pi^0 K^0) &= -4\mathrm{Im}(\lambda_u^* \lambda_t)\mathrm{Im}\left[(P_{uc} - C)^* \left(P_{tc} - P_{\rm EW} - \frac{1}{3}P_{\rm EW}^C\right)\right], \\
\Delta(\pi^+ K^0) &= -4\mathrm{Im}(\lambda_u^* \lambda_t)\mathrm{Im}\left[(A + P_{uc})^* \left(P_{tc} - \frac{1}{3}P_{\rm EW}^C\right)\right].
\end{aligned} \tag{14}$$

The direct CP asymmetry $A_{CP}(\pi K)$ is subsequently defined as

$$A_{CP}(\pi K) = \frac{\Delta(\pi K)}{\Gamma(b) + \Gamma(\bar{b})}, \tag{15}$$

For B^0 and $\overline{B^0}$ decaying to the CP-eigenstate $f_{\rm CP}$, one may also measure the mixing-induced CP violation, parametrized by S_{CP} and defined as

$$A_{CP}(t) = \frac{\Gamma(\overline{B^0}(t) \to f) - \Gamma(B^0(t) \to \bar{f})}{\Gamma(\overline{B^0}(t) \to f) + \Gamma(B^0(t) \to \bar{f})} = A_{CP}(f)\cos(\delta m t) + S_{CP}(f)\sin(\delta m t) \tag{16}$$

where $\delta m = m_H - m_L$ is the mass difference between the heavier and lighter B-meson mass eigenstates. By ignoring diagrams of $\mathcal{O}(\lambda^2)$ and beyond, the $B \to \pi K$ amplitudes reduce to

$$\begin{aligned}
\mathcal{A}^{-+} &= -\lambda_u T - \lambda_t P_{tc}, \\
\mathcal{A}^{+0} &= \lambda_t P_{tc}, \\
\sqrt{2}\mathcal{A}^{00} &= \lambda_t (P_{tc} - P_{\rm EW}), \\
\sqrt{2}\mathcal{A}^{0+} &= -\lambda_u T - \lambda_t (P_{tc} + P_{\rm EW}).
\end{aligned} \tag{17}$$

Direct CP asymmetries in $B^0 \to \pi^- K^+$ and $B^+ \to \pi^0 K^+$ arise because of the T—P_{tc} interference leading to a nonzero relative strong phase, as well as a weak phase difference between the two topological amplitudes. In contrast, $P_{\rm EW}$ and T carry the same strong phase as they are related by a real number as shown in Eq. (12). Therefore, $P_{\rm EW}$—T interference for $B^+ \to \pi^0 K^+$ does not contribute to A_{CP}. Thus, one expects a simplified relation [19],

$$A_{CP}(B^0 \to \pi^- K^+) = A_{CP}(B^+ \to \pi^0 K^+). \tag{18}$$

Any deviation, numerically expressed by the quantity Δ_{CP},

$$\Delta A_{CP} = A_{CP}(B^+ \to \pi^0 K^+) - A_{CP}(B^0 \to \pi^- K^+), \tag{19}$$

thus, would necessarily mean that amplitudes like C may not be neglected, but it would be very premature to claim this as a telltale signature of NP. A more robust CP sum rule relation [71] connecting all the four $B \to \pi K$ CP asymmetries, namely,

$$A_{CP}(\pi^-K^+)+A_{CP}(\pi^+K^0)\frac{\mathcal{B}(\pi^+K^0)\tau_0}{\mathcal{B}(\pi^-K^+)\tau_+} =A_{CP}(\pi^0K^+)\frac{2\mathcal{B}(\pi^0K^+)\tau_0}{\mathcal{B}(\pi^-K^+)\tau_+}+A_{CP}(\pi^0K^0)\frac{2\mathcal{B}(\pi^0K^0)}{\mathcal{B}(\pi^-K^+)}, \tag{20}$$

holds up to a few percent where $\mathcal{B}(\pi K)$ are the BRs and τ_+ and τ_0 are the lifetimes of B^+ and B^0 mesons respectively. While deriving Eq. (20), it was assumed that the annihilation amplitude A is suppressed relative to color-allowed tree amplitude T and the relative strong phase difference between the T and C amplitudes is small. The algebraic relation, Eq. (11), between tree and EWP amplitudes was also used. A deviation from the sum rule in Eq. (20) is quantified by an observable Δ_4,

$$\Delta_4 = A_{CP}(\pi^-K^+) + A_{CP}(\pi^+K^0)\frac{\mathcal{B}(\pi^+K^0)\tau_0}{\mathcal{B}(\pi^-K^+)\tau_+} - A_{CP}(\pi^0K^+)\frac{2\mathcal{B}(\pi^0K^+)\tau_0}{\mathcal{B}(\pi^-K^+)\tau_+} - A_{CP}(\pi^0K^0)\frac{2\mathcal{B}(\pi^0K^0)}{\mathcal{B}(\pi^-K^+)}, \tag{21}$$

so that $\Delta_4 \neq 0$ may be considered as a strong hint for NP. It has been shown in Ref. [56] that NP contributions in $B \to \pi K$ decays can be absorbed by reparametrizing the SM amplitudes, so that NP effects may be hidden. However, observables like ΔA_{CP} and Δ_4 are not invariant under such reparametrization.

III. METHODOLOGY

The goal of the numerical analysis would be to find out the posterior distribution (parameter space) of the various amplitudes and their corresponding relative phases, allowed by the data. The available data consist of four BRs for the $B \to \pi K$ modes, four direct CP asymmetries ($A_{\rm CP}$), and the mixing-induced CP asymmetry S_{CP} measured for the $B \to \pi^0 K^0$ decay. Instead of using the averages quoted in [74], we utilize all the available data

TABLE I. Experimental inputs used in this work. The first uncertainty is statistical and the second one is systematic.

Modes	Experiment	BR $[10^{-6}]$	Experiment	$A_{\rm CP}$	$S_{\rm CP}$
$B^0 \to \pi^-K^+$	*BABAR* [5]	19.1(6)(6)	*BABAR* [9]	$-0.107(16)(^{6}_{4})$	
	Belle [11]	20.00(34)(60)	Belle [11]	−0.069(14)(7)	
	CLEO [75]	$18.0(^{23}_{21})(^{12}_{9})$	CDF [76]	−0.083(13)(4)	
			LHCb [13]	−0.084(4)(3)	
			LHCb [14]	−0.0824(33)(33)	
	Belle-II [15]	18.0(9)(9)	Belle-II [15]	−0.16(5)(1)	
$B^+ \to \pi^0K^+$	*BABAR* [7]	13.6(6)(7)	*BABAR* [7]	0.030(39)(10)	
	Belle [11]	12.62(31)(56)	Belle [11]	0.043(24)(2)	
	CLEO [75]	$12.9(^{24}_{22})(^{12}_{11})$	LHCb [18]	0.025(15)(6)	
	Belle-II [16]	$11.9(^{10}_{11})(^{11}_{16})$	Belle-II [16]	−0.09(9)(3)	
$B^+ \to \pi^+K^0$	*BABAR* [6]	23.9(11)(10)	*BABAR* [6]	−0.029(39)(10)	
	Belle [11]	23.97(53)(71)	Belle [11]	−0.011(21)(6)	
	CLEO [75]	$18.8(^{37}_{33})(^{21}_{18})$	LHCb [12]	−0.022(25)(10)	
	Belle-II [15]	$21.4(^{23}_{22})(16)$	Belle-II [15]	−0.01(8)(5)	
$B^0 \to \pi^0K^0$	*BABAR* [9]	10.1(6)(4)	*BABAR* [8,77]	−0.13(13)(3)	0.55(20)(3) [8,77]
	Belle [10]	8.7(5)(6)	Belle [10,77]	0.14(13)(6)	0.67(31)(8) [10,77]
	Belle [11]	9.68(46)(50)			
	CLEO [75]	$12.8(^{40}_{33})(^{17}_{14})$			
	Belle-II [17]	$8.5(^{17}_{16})(12)$	Belle-II [17]	$-0.40(^{46}_{44})(4)$	

that are used to calculate those averages for the fits and show them in Table I. Very recent results from Belle-II [15–17] are also included in this analysis. Without neglecting any contribution from diagrams up to $\mathcal{O}(\lambda^3)$, we have ten free parameters: the 5 magnitudes P_{tc}, $|T|$, $|C|$, $|A|$, $|P_{uc}|$, four relative phases $\delta_T, \delta_C, \delta_A, \delta_{P_{uc}}$, and the parameter κ, which we have chosen, at times, to vary as a free parameter instead of fixing it to the SM expectation. We have defined the relative phases with respect to the P_{tc} diagram whose absolute phase is set to zero in this convention [39].

Let us explain the rationale for using all the data points for an observable, and not their quoted average. First, the quoted averages do not include all the latest results from LHCb and Belle-II. Secondly, a correct averaging should implement all statistical and systematic correlations between the data points, which we do not have at our disposal. Thus, we are forced to perform our own averaging, which involves the creation of a negative log-likelihood using all data points. This is precisely what we do in our analysis, with the observables replaced by their parametric theoretical expressions.

In the next section we talk about our fits. Among the six fits performed in this paper, only two *Order-3* fits have nine and ten free parameters. For the rest, the number of free parameters is six or seven; an analysis with only the averages would have been perfectly possible for all of them, and even a frequentist fit would have been meaningful. Though a numerical minimization of a cost function (negative log-likelihood or χ^2) can always be done with an arbitrary number of parameters and a best fit can be obtained, interpretation of that result (when the number of free parameters is more than the number of data points) from a frequentist point of view is dicey, as effective degrees of freedom become unphysical. From a Bayesian point of view, however, this just means that the posteriors are unconstrained. We will show that this is exactly what we find for our *Order-3* fits, whose posteriors have more than optimal variance.

Though we mainly follow a Bayesian framework for the purpose of the present analysis, we also simultaneously follow the frequentist interpretations of our results, whenever possible. This means that in addition to the obtained

TABLE II. Central tendency (Median) and uncertainties ($1\sigma \equiv 68.27\%$ credible intervals around the central estimates) for fits with one distinct high-probability region. Notably, uncertainty propagation using these parameters uses the whole sample from the posterior, not these point estimates. Parameters in the lower part of the table are used as priors in the fits. The topological amplitudes are defined by factoring out $G_F/\sqrt{2}$ and therefore the amplitudes are given in units of $(\mathrm{GeV})^3$.

		Real κ				Complex κ
		SM (κ Prior)		κ Free		
Parameters	Priors	Order-2	Order-3	Order-2	Order-3	Order-2
κ	0.014(6)	$0.0210(^{44}_{43})$	$0.0210(^{44}_{43})$	$0.028(^{41}_{14})$	$0.029(^{47}_{14})$	$0.048(^{80}_{28})$
P_{tc}	…	$-0.1524(^{62}_{65})$	$-0.1524(^{61}_{66})$	$-0.1551(^{66}_{69})$	$-0.1548(^{72}_{70})$	$-0.1534(^{78}_{74})$
$\lvert\mathrm{T}\rvert$	…	$0.486(^{11}_{22})$	$0.486(^{11}_{22})$	$0.49(^{28}_{15})$	$0.49(^{29}_{16})$	$0.68(^{22}_{24})$
$\lvert\mathrm{C}\rvert$	…	$0.23(^{11}_{18})$	$0.23(^{12}_{18})$	$0.454(^{150}_{83})$	$0.471(^{166}_{94})$	$0.58(^{22}_{16})$
δ_κ	…	…	…	…	…	$0.70(^{71}_{50})$
$\lvert\mathrm{A}\rvert$	…	…	$0.0051(^{34}_{35})$	…	$0.047(^{35}_{32})$	…
$\lvert P_{\mathrm{uc}}\rvert$	…	…	0.0050(34)	…	$0.049(^{35}_{33})$	…
δ_T	…	$3.724(^{59}_{49})$	$3.724(^{59}_{51})$	$3.75(^{37}_{24})$	$3.71(^{37}_{23})$	$3.48(^{29}_{40})$
δ_C	…	$1.37(^{23}_{22})$	$1.36(^{23}_{22})$	$1.03(^{26}_{34})$	$1.02(^{26}_{37})$	$0.74(^{540}_{33})$
δ_A	…	…	$2.7(^{28}_{18})$	…	$3.7(^{17}_{26})$	…
$\delta_{P_{\mathrm{uc}}}$	…	…	$3.3(^{20}_{23})$	…	$3.9(^{16}_{24})$	…
$\lvert V_{\mathrm{us}}\rvert$	0.2245(8)	$0.22455(^{80}_{81})$	0.22456(80)	0.2245(8)	0.22449(80)	0.22451(80)
$\lvert V_{\mathrm{ub}}\rvert$	0.0038(2)	0.00407(23)	0.00407(23)	0.00382(24)	0.00381(24)	0.00383(24)
$\lvert V_{\mathrm{tb}}\rvert$	1.01(3)	1.016(30)	1.015(30)	1.011(30)	1.011(30)	1.011(30)
$\lvert V_{\mathrm{ts}}\rvert$	0.039(1)	0.0389(11)	0.0389(11)	0.0387(11)	0.0387(11)	0.0387(11)
γ	1.26(7)(8)	1.247(91)	$1.246(^{92}_{91})$	1.24(11)	1.24(11)	1.24(11)
β	0.39(1)(1)	0.385(17)	0.385(17)	0.386(17)	0.386(17)	0.386(17)

parameter posteriors and the corresponding estimates of central tendency and dispersion, we also keep track of the maximum likelihood estimates (MLEs), corresponding fit-probabilities (in terms of p-values) and one-dimensional confidence levels (CLs). In the Appendix, we attach a glossary for the Bayesian terms used here.

Apart from the free parameters, the magnitude of the CKM elements $|V_{ub}|$, $|V_{us}|$, $|V_{tb}|$, $|V_{ts}|$, and the CKM angles β and γ, come into the analysis as uncertain theoretical inputs coinciding with latest Heavy Flavour Averaging Group averages [78]. They are incorporated as multinormal priors, details of which are provided in the lower part of the second column of Table II. The effect of the uncertainties of meson masses and the B-meson lifetimes are very small compared to the other sources of uncertainties and are thus neglected in the present analysis.

(a) Details of Frequentist fit-procedure: Finding the MLE of the parameters boils down to minimizing the quantity $\chi^2 \equiv -2\ln(\mathcal{L})$ with respect to the parameters, where $\mathcal{L}$ is the likelihood for the experimental observations. For Gaussian data, it simplifies to the actual form of a χ^2 function. Except particular S_{CP} and A_{CP} measurements in *BABAR* and Belle which are correlated [77], the experimental inputs are independent and we incorporate that correlation in our analysis. Whenever applicable, we take average of the asymmetric uncertainties. One may note that the frequentist fits make sense only for the *Order-2* fits described in the next section.

(b) Details of the Bayesian analysis: CKM parameters come into the analysis as theoretical inputs and as mentioned above, we use their measured values as multinormal priors. For all other parameters, uniform priors are supplied in a wide range. Using the log-likelihood ($\ln\mathcal{L}$) and the priors, we sample the unnormalized log-posterior by running a Markov Chain Monte Carlo (MCMC) process. We follow the Metropolis-Hastings algorithm [79] with a multinormal proposal distribution for the MCMC runs. Convergence of the first quartile is ensured using single-chain diagnostics like Raftery-Lewis [80] and thinned samples are used to reduce the autocorrelation of the chain.

Our results on the allowed parameter spaces are shown, for clarity, as two-dimensional Bayesian fits. The fits have been organized on two factors; the relationship of the EWP amplitudes to T and C amplitudes, and the number of parameters considered for the fit.

(a) The relationship shown in Eq. (11) holds to a very good extent in the SM, leading to a single κ parameter. It may not actually be so when NP is present, e.g., there can be two such parameters, $P_{\rm EW} \sim \kappa_1 T$ and $P^C_{\rm EW} \sim \kappa_2 C$. This case, and the case with κ as a complex parameter, have been considered in detail. Such options are, of course, not SM-like.

(b) Among the ten free parameters, two amplitudes, namely, $|A|$ and $|P_{uc}|$, are expected to be small ($\sim\lambda^3$), and hence the exact values of their phases, δ_A and $\delta_{P_{uc}}$ respectively, are expected to be irrelevant. For all the cases of κ discussed earlier, we have performed two sets of fits; one with all the nine parameters (plus κ), which we call *Order-3* fits, and one excluding the four parameters mentioned above, which we call *Order-2* fits.

The rationale for all these fits and the final results follow in Sec. IV. By letting the parameters vary over a large range (not necessarily consistent with SM), we ensure to get the correct global picture of the potentially complicated multidimensional probability landscape of the parameters.

IV. RESULTS

We will show our results for six different fits, as follows:

(i) *Order-2*, with a single real κ as a free parameter;
(ii) Same as (i) but at *Order-3*;
(iii) *Order-2*, with a single real κ as a given normal prior (0.014 ± 0.006), and with the extra constraint $|C| \leq |T|/2$;
(iv) Same as (iii) but at *Order-3*;
(v) *Order-2*, with a single complex $\kappa = |\kappa|\exp(i\delta_\kappa)$ as a free parameter;
(vi) *Order-2*, with two real κ-type free parameters, κ_1 and κ_2.

Let us first summarize the main points of this section:

(1) The *Order-2* fit with a single real κ as a given prior produces a perfectly acceptable fit in the SM-like region. When κ is treated as a free parameter, the best-fit region is found to have a large overlap with the SM-like parameter space.
(2) The *Order-3* fits do not improve over the *Order-2* fits. In other words, *Order-2* seems to be the optimal choice at the present experimental precision.
(3) The predictions for ΔA_{CP} and Δ_4 are mutually consistent for all the fits.
(4) The fit with two real κ parameters shows some interesting features while keeping the above conclusions more or less intact, but this definitely falls under NP.

We will now quantify these qualitative remarks.

A. Order-2 fits

Let us start with fit (i), i.e., the *Order-2* fit with three independent amplitudes, two phases, and κ. Just to cross-check with the frequentist approach, we find that the high-probability region of the parameter posterior distribution of the Bayesian analysis also contains the frequentist best-fit corresponding to a very high p-value.

The point estimates of the central tendency and dispersion of the parameters [medians with 1σ credible intervals (CI) around them] are listed in the fifth column

of Table II [*Real κ (Free) Order-2*]. The 2D marginal-posteriors of the parameters are shown in Figs. 2(b)–2(f) as reddish constant probability contours with increasing probability content (from lighter to darker), and as their bluish versions in Figs. 3 and 4.

A rather naive *Order-2* SM fit was performed first, setting the free parameters to vary within the following bounds:

$$0 \le \kappa \le 0.03, \qquad -0.3 \le P_{tc} \le 0,$$
$$0 \le |T| \le 0.5, \qquad 0 \le |C| \le 0.1. \tag{22}$$

We find that there is no acceptable fit in this region (p-value $< 1\%$). This holds true even if we extend the analysis to *Order-3* and scan the four additional parameters in the following way

$$0 \le |A| \le 0.01, \qquad 0 \le |P_{uc}| \le 0.01,$$
$$0 \le \delta_A \le 2\pi, \qquad 0 \le \delta_{P_{uc}} \le 2\pi. \tag{23}$$

In other words, such a naive-SM parameter space is definitely ruled out by the data.

Next, we focus on κ and C, and take some leeway from the naive estimates. Using the approximate value of κ mentioned in Sec. II A, we use a normal prior for κ in the fit, with the same median, but five times the uncertainty [fit (iii)]. This prior is mentioned in the second column of Table II. Throughout this fit, we use the following additional constraints,

$$-0.3 \le P_{tc} \le 0, \qquad 0 \le |T| \le 0.5, \qquad |C| \le (|T|/2), \tag{24}$$

i.e., the tight $|C| < 0.1$ being relaxed without jeopardising the SM expectation for the ratio. It can, therefore, be argued, that any allowed parameter space we find in this region, may safely be labelled SM-like. Let us call this the *SM-like κ-prior Order-2* fit. In a frequentist fit, this corresponds to a quite acceptable p-value. The medians of the 1D-marginals with 1σ CIs around them are listed in the third column of Table II. The constant (red) probability contours enclosing respectively the 68.28% (solid) and 95.45% (dot-dashed) CIs are shown as 2D marginal posteriors (with contours enclosing gradually increasing total probability-content from darker to lighter) in all the plots of Figs. 3 and 4. As expected, this parameter space has some overlap with that of the real κ *Order-2* fit. Similar 2D marginals containing the parameter κ are shown with similar purple contours in Fig. 2.

In the next stage, we consider fit (vi), i.e., two parameters κ_1 and κ_2 instead of a single κ and perform the *Order-2* fit. From the frequentist result, we find two distinct minima here (one deeper than the other): one where $\kappa_1 \sim \kappa_2$ and another where κ_2 is considerably larger than κ_1. For both best fits, κ_1-values are similar, and both are excellent fits. As can be seen from Figs. 2(a) and 2(b), the Bayesian posteriors [in Fig. 2(a), blue solid (68.28%) and dot-dashed (95.45%) contours; in Figs. 2(b)–2(f), same for κ_1 and green dashed (68.28%) and dotted (95.45%) contours for κ_2] are consistent with this finding.

Let us note here the ranges over which fit-parameters other than κ are scanned, which clearly highlight the beyond-SM nature of the parameter space,

$$-0.3 \le P_{tc} \le 0, \qquad 0 \le |T| \le 1, \qquad 0 \le |C| \le 1,$$
$$0 \le \delta_T \le 2\pi, \qquad 0 \le \delta_C \le 2\pi. \tag{25}$$

From Figs 2 and 3, one may see that there are two distinct high probability regions, separated at 1σ but connected at higher σs in the $P_{\rm tc}$ direction, in the parameter space. The actual best fit in Bayesian approach has considerable overlap with the SM-like region of the single real κ fit, except for the parameter $|C|$. This is evident from Figs. 2(d), 3(b), 3(e), 4(c), and 4(d), where the agreement is seen to be at $\sim 2\sigma$. One may note the physics behind this. The SM-like parameter-space is actually very skewed, due to the abrupt cut that we had imposed on $|C|$ and $|T|$ ($|T| \le 0.5$ and $|C| \le (|T|/2)$). Relaxing both these constraints even slightly should naturally include a higher-probability parameter space. Following the discussion in Section II A, we see that such possibilities may not be entirely ruled out, in which case these regions, can, in turn, be completely consistent with those for the free real κ case. The other high probability region (containing the actual maximum likelihood estimate from the frequentist fit) is clearly far away from the SM expectations for the amplitudes. Where κ_1 shares most of its high-probability parameter space with that of the single real κ, a set of quite large values of κ_2 are allowed in the nonstandard region. A significant variation of κ from Eq. (12) indicates that the WCs for the EWP operators are enhanced from their SM values, most probably because of NP.

If we vary P_{tc} to include positive values as well, we will get a disjointed but identical parameter space symmetric about $P_{tc} = 0$. Since the strong phase of P_{tc} is set to zero and the rest of the phases are defined relative to it, this sign ambiguity should be resolved by keeping only the positive or negative set of values of P_{tc}. We chose the negative part of the parameter space arbitrarily.

We can go further, consider fit (v), i.e., take κ to be a complex parameter $\kappa = |\kappa| \exp(i\delta_\kappa)$ for the sake of the analysis, and repeat fit (i). The constant (blue) probability contours enclosing respectively the 68.28% (solid) and 95.45% (dot-dashed) credible regions in 2D marginal posteriors in the $|\kappa|$–δ_κ plane are shown in Fig. 5(c), where δ_κ is equivalent to the relative strong phase between tree and electroweak penguin amplitudes, and is expected to be close to zero [64,67]. Due to this, unlike the other phases occurring in this analysis, the prior for δ_κ is set to be a

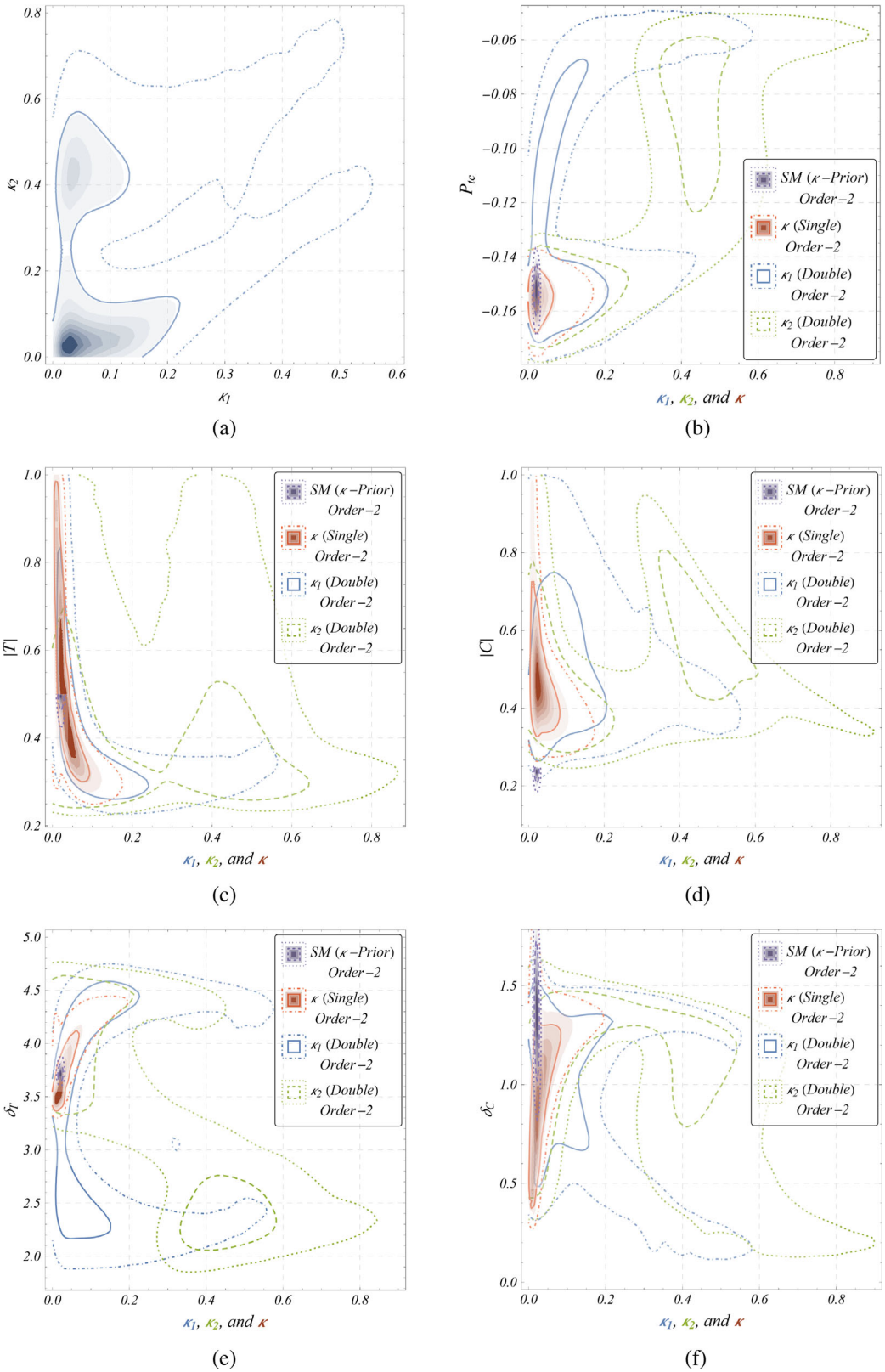

FIG. 2. Marginal posteriors (2D) with constant probability contours. In Fig. 2(a), contours enclose 68.28% (blue, solid) and 95.45% (blue, dot-dashed) CIs. Those in the rest of the figures are for κ_1 vs the corresponding parameter in the y-axis, while green ones, dashed and dotted, represent the κ_2 marginals. The reddish brown contours with changing opacity enclose regions with decreasing probability (from darker to lighter) for the *Order-2* fit with a single real κ. (a) $\kappa_1 vs\, \kappa_2$ (b) $\kappa_1, \kappa_2$and $\kappa\ vs\ P_{tc}$ (c) $\kappa_1, \kappa_2$and $\kappa\ vs |T|$ (d) $\kappa_1, \kappa_2$and $\kappa\ vs |C|$ (e) $\kappa_1, \kappa_2$and $\kappa\ vs\ \delta_T$ (f) $\kappa_1, \kappa_2$and $\kappa\ vs\ \delta_C$.

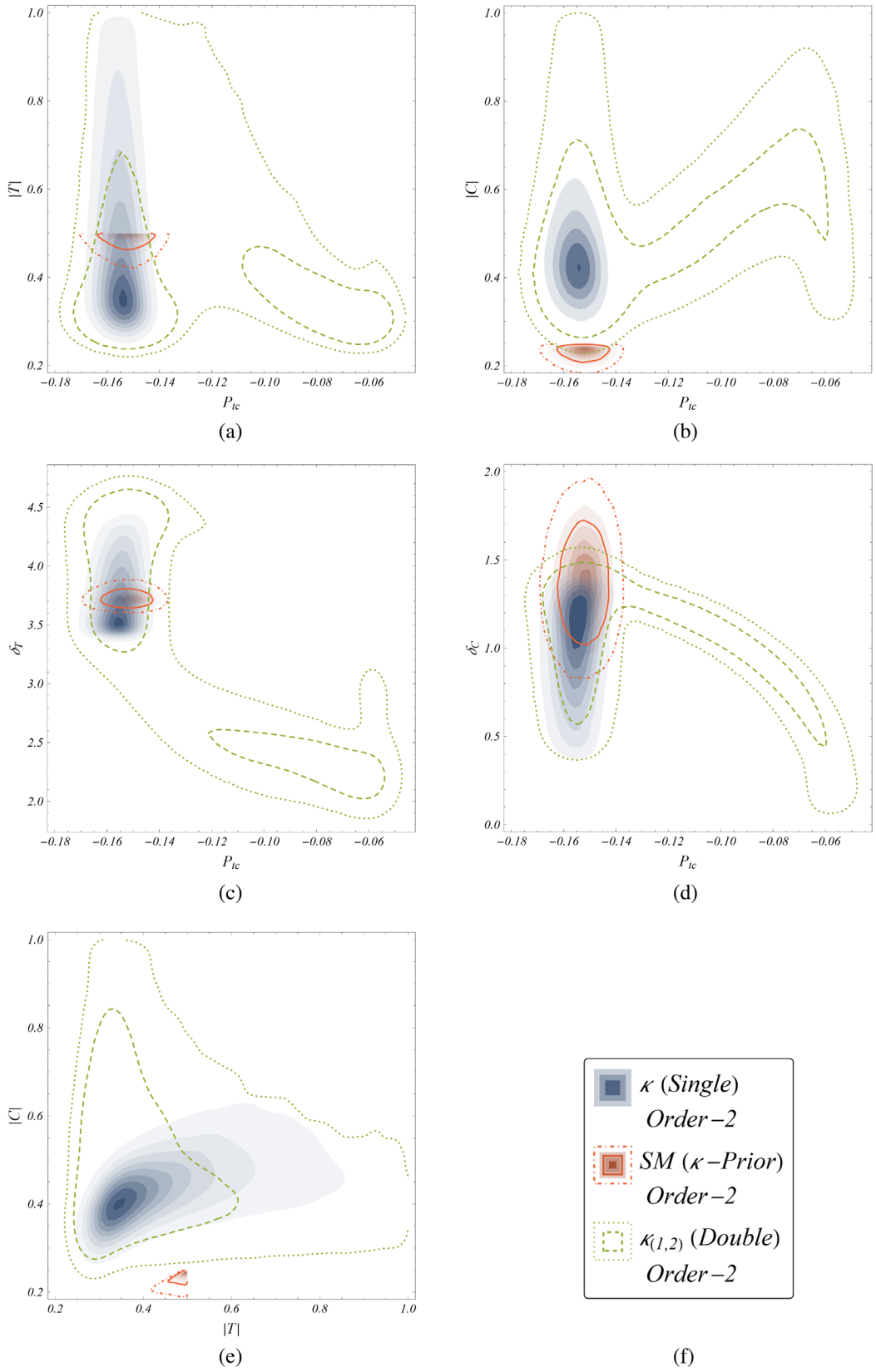

FIG. 3. Marginal posterior distributions (2D) with constant probability contours. Green dashed (dotted) contours represent the 68.28% (95.45%) CIs for the *Double-*κ *Order-2* fit, while red (solid, dot-dashed) contours denote those of the *κ-Prior Order-2* fit. The bluish contours with changing opacity enclose the high probability regions with decreasing probability (from darker to lighter) for the *Single real* κ *Order-2* fit. (a) $P_{tc}vs|T|$ (b) $P_{tc}vs|C|$ (c) $P_{tc}vs\,\delta_T$ (d) $P_{tc}vs\,\delta_C$ (e) $|T|\,vs\,|C|$ (f) Legend.

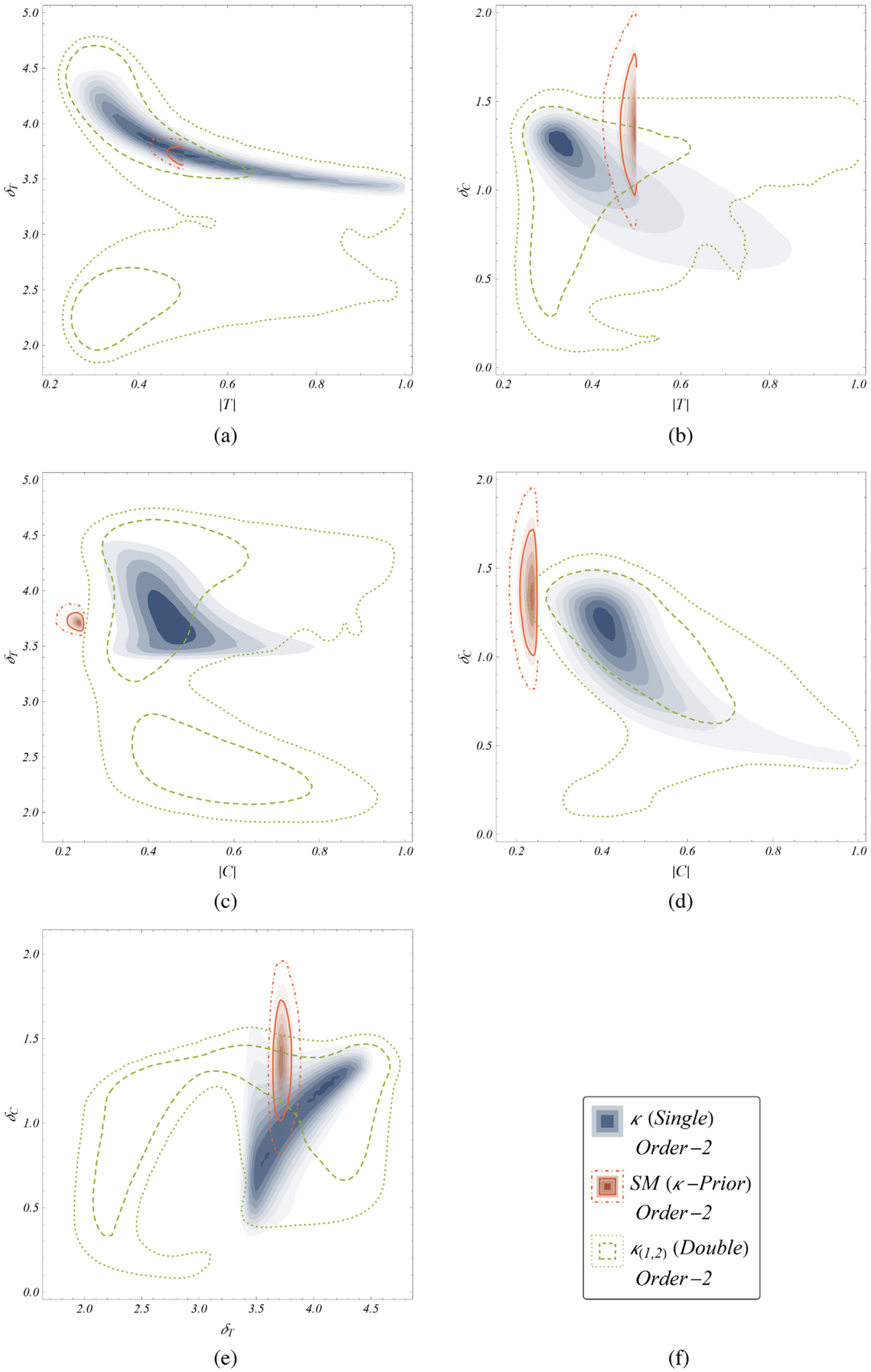

FIG. 4. Continued from Fig. 3. (a) $|T|vs\,\delta_T$ (b) $|T|vs\,\delta_C$ (c) $|C|vs\,\delta_T$ (d) $|C|vs\,\delta_C$ (e) $\delta_T\,vs\,\delta_C$ (f) Legend.

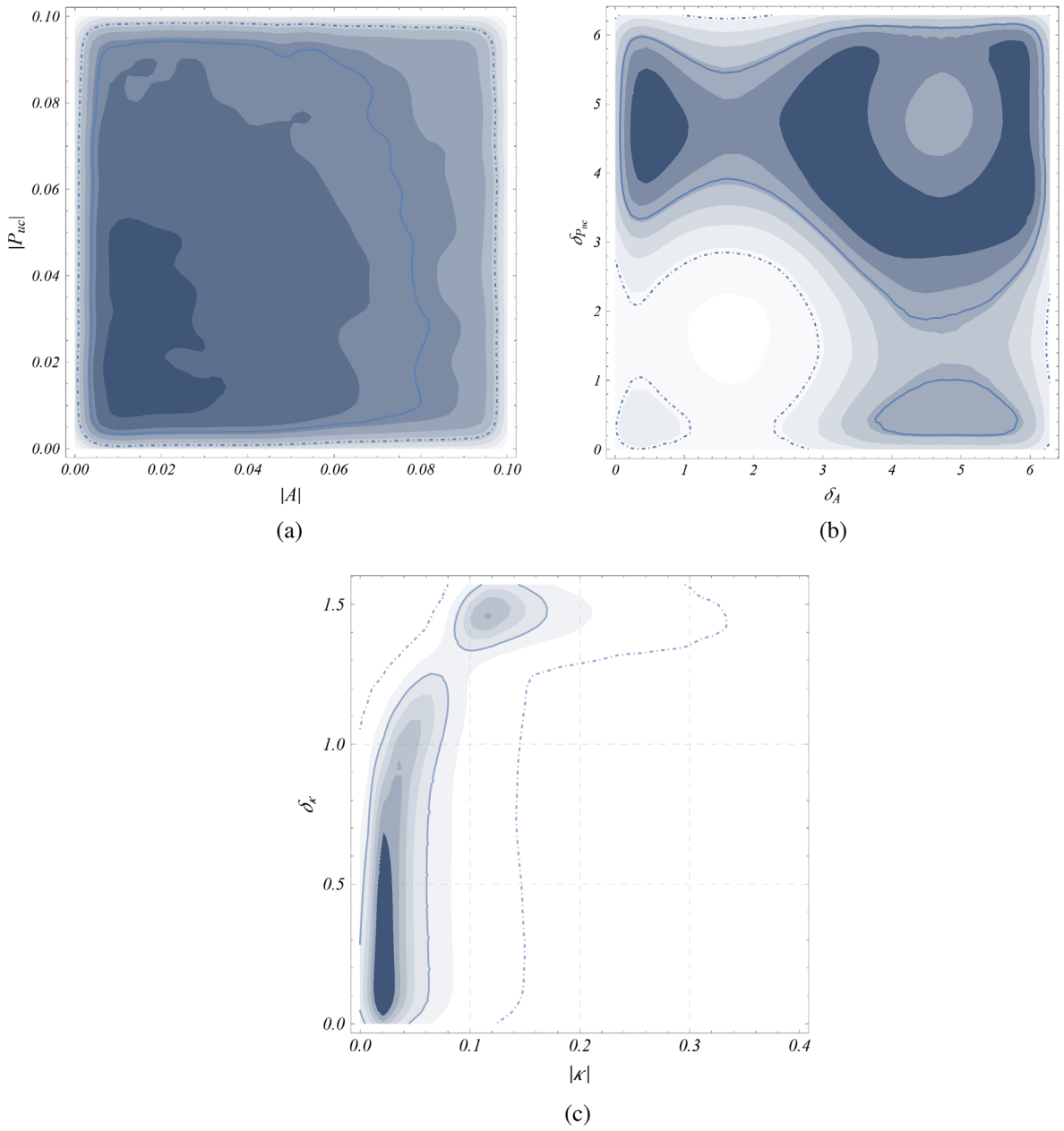

FIG. 5. 2D marginal posteriors similar to Fig. 2. First two figures are for the extra four parameters for the *Single Real κ Order-3 Fit*. The last one is the $|\kappa|$–δ_κ plane for the *Complex κ Order-2 Fit*. (a) $|A| vs |P_{uc}|$ (b) δ_A *vs* $\delta_{P_{uc}}$ (c) $|\kappa| vs\, \delta_\kappa$.

uniform distribution $0 \le \delta_\kappa \le \frac{\pi}{2}$. The central tendency and dispersion of the posterior parameter space is depicted in the last column of Table II in terms of the median and 1σ CIs around it. It is evident that the best-fit solution is consistent with $\delta_\kappa = 0$.

B. Order-3 fits

We can perform an analogous exercise, i.e., fits (ii) and (iv), taking into account the four parameters neglected so far, and scanning them over the range

$$0 \le |A| \le 0.1, \qquad 0 \le |P_{uc}| \le 0.1,$$
$$0 \le \delta_A \le 2\pi, \qquad 0 \le \delta_{P_{uc}} \le 2\pi. \tag{26}$$

As we pointed out earlier, a frequentist *Order-3* fit is questionable, and a Bayesian fit leads to unconstrained posteriors.

In other words, we expect the newly introduced $\mathcal{O}(\lambda^3)$ parameters to be very imprecise and the amplitudes to be consistent with zero. This is supported from the corresponding entries of the sixth column of Table II [*Real κ (Free)*

Order-3] as well as from Figs. 5(a) and 5(b), which show the 2D marginal-posteriors of the higher-order parameters as reddish constant probability contours. Though apparently the highest probability regions are close to zero, note that we have only scanned these amplitudes up to 0.1, and observe a more or less flat nature of the 1D posterior in that region. We refrain from showing the posteriors for the other parameters, as they are very similar to those of *Order-2* fits, with only a slight increase in spread for some parameters.

The posterior medians with 1σ CIs for fit (iv), *SM-like* (κ-*prior*) *Order-3*, are listed in the fourth column of Table II. The *Order-2* fits being quite optimal at the present level, we have not tried the *Order-3* analogs for fits (v) and (vi), i.e., with a complex κ and with two real κs.

At this point, a few comments on the fit results are in order. From the unconstrained fit, we see that for the best-fit region, the color-suppressed tree amplitude $|C|$ is enhanced and is of the same order of magnitude as the color-allowed tree amplitude $|T|$, resulting in $0.7 < |C|/|T| < 1$ for all the fits in Table II, except the SM-like fits, where we had specifically set $|C|/|T| < 0.5$. This is consistent with the predictions from specific model calculations [32,34] for the topological amplitudes. On the other hand, where soft collinear effective theory based approaches predict $\mathrm{Arg}(C/T) \sim 0$ [32], a quite large value of $\mathrm{Arg}(C/T)$ ($\sim 200°$) is found to be favored in the previous $B \to \pi K$ fits [44]. Nonzero values of $\mathrm{Arg}(C/T)$ are also expected from global analysis of B decays to two pseudoscalar mesons [81]. As can be seen from Table II, for all fits with free κ and no constraint on $|C|/|T|$, $\mathrm{Arg}(C/T) \sim -2.7 \approx 205°$, making our results consistent with the earlier $B \to \pi K$ fits. For the constrained SM-like fits, $\mathrm{Arg}(C/T) \sim -2.35 \approx 225°$.

C. Predictions

Before we talk about predictions of observables, namely, ΔA_{CP} and Δ_4, the reader may note that the global average of the observable ΔA_{CP}, defined in Eq. (19) and quoted in the introduction [18], does not contain the latest results from Belle-II, as the latter results came after the publication of Ref. [18]. Also, the only measurement of the observable Δ_4, defined in Eq. (21), can be found in Ref. [11], which is almost a decade old. We have thus used the results listed in Table I and found the global averages of the observables and in turn, that of ΔA_{CP} and Δ_4. The results are

$$\Delta A_{CP}^{\mathrm{global}}(\pi K) = 0.112 \pm 0.013,$$
$$\Delta_4^{\mathrm{global}}(\pi K) = -0.122 \pm 0.097, \qquad (27)$$

with correlation $= -0.175$. From here onwards, whenever we mention the global average of these observables, we will mean these numbers.

We mentioned earlier that ΔA_{CP} is expected to be zero in SM [19] and the main goal of the present work is to check the robustness of that claim. The rationale for this claim is

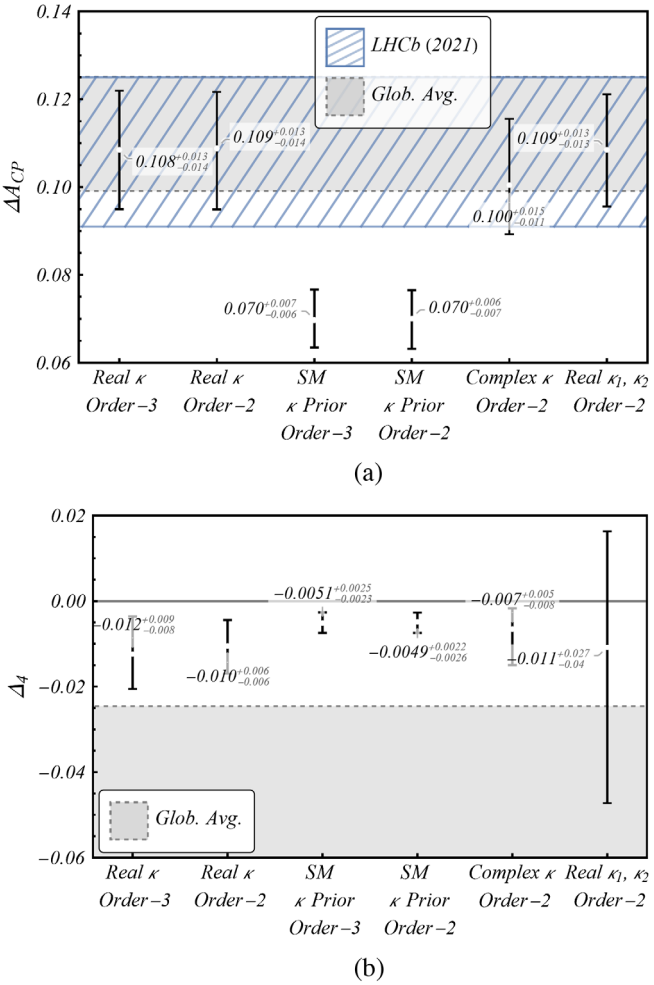

FIG. 6. The predicted 1D distributions of observables ΔA_{CP} and Δ_4. Figure 6(a) compares various predictions of ΔA_{CP} with experiment, while Fig. 6(b) does the same for Δ_4.

the expected smallness of C and the expected small value of $\mathrm{Arg}(C/T)$. Once these two assumptions are relaxed, which still does not take us beyond the SM, ΔA_{CP} need not be small. As has been shown in the earlier sections, the favored parameter spaces for most of the parameters are consistent with their respective SM expectations within 2σ. Using the extended sample of the posteriors of these fits, we can find the predicted distributions of ΔA_{CP} and Δ_4. Figure 6(a) compares the predicted values of ΔA_{CP} with the global average, as well as the recent LHCb measurement [18]. We have used the mode (*maximum a posteriori*) and 1σ high-density CIs around them in showing the predicted distributions of the observables. We see that both real κ (unconstrained) fits yield very similar values of Δ_{CP}. The complex κ fit provides slightly shifted, but completely consistent results. For the SM-like fits with κ as a prior, Δ_{CP} is smaller than the global average. The central result is that the predictions for these SM-like fits are more than 5σ away from zero but are consistent with both the LHCb result

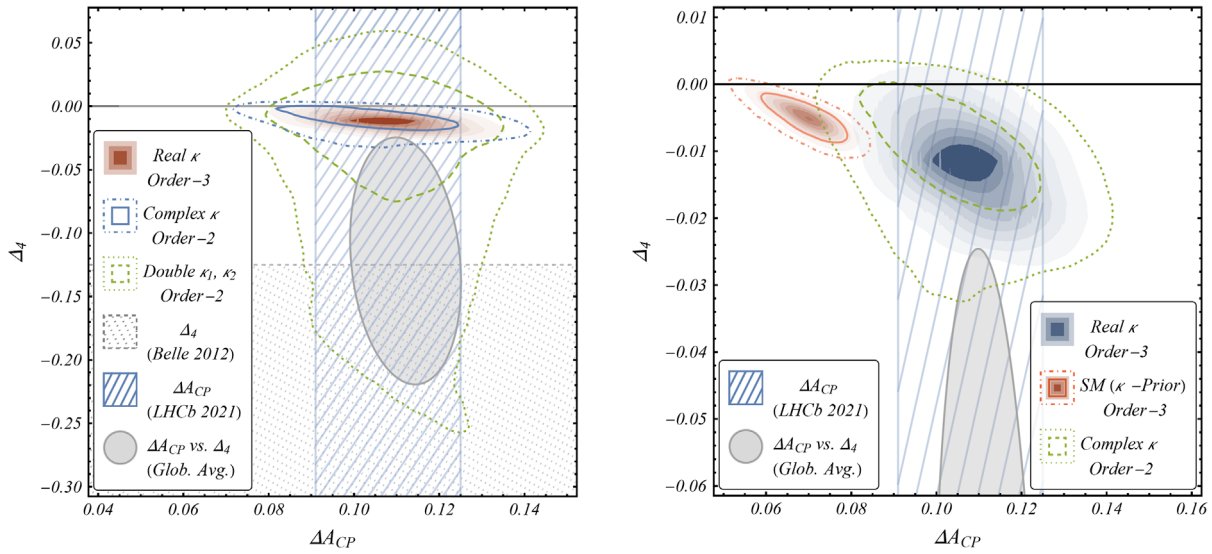

FIG. 7. The predicted combined distributions of observables $\Delta A_{\rm CP}$ and Δ_4. Figure 7(a) compares the experimental results with predicted combined distributions in the $\Delta A_{\rm CP}$–Δ_4 plane for various fit results. Figure 7(b) zooms in to the predicted distributions from several fits. The first (second) figure exclusively contains the *Double-κ Order-2* (*SM-like κ-Prior Order-3*) fit. All experimental bands and error ellipses denote only 1σ confidence intervals.

and the global average within 2σ. This shows that the data, though not completely consistent with the SM yet, is nowhere near the assumed large deviation of $\sim 8\sigma$.

The case of Δ_4, as seen in Fig. 6(b), is more interesting. First of all, except the *Double-κ Order-2* fit, none of the predictions are consistent with either zero or the global average within 1σ, though they are quite close to that. The biggest uncertainty comes from the Double-κ fit. This prediction contains both the high-probability regions of the corresponding posterior.

Figure 7 shows the correlation between Δ_{CP} and Δ_4. One may note that the global average ellipse is only at 1σ, so none of the fits show any serious tension. However, if a more precise measurement unambiguously points to a negative definite value of Δ_4, the Double-κ fit will be favored, which definitely indicates NP. Thus, we conclude that along with ΔA_{CP}, Δ_4 too may act as an indicator for NP, or some new SM dynamics. Moreover, as can be seen from the varying uncertainties of the predictions in Fig. 6(b), it may differentiate among all these possibilities.

V. DISCUSSION

In this paper, we have critically analyzed the data on all the $B \to \pi K$ modes coming from all experiments, and checked how far the claim of an 8σ tension between the global average of $\Delta A_{\rm CP}$ and its SM expectation can be sustained. Thanks to all the independent experiments, there is no scarcity of data, and the fitting procedure, as outlined previously, makes sense. What we find is more or less on the expected line:

(i) If we take a very naive estimate of the SM topological amplitudes, as dictated by the CKM elements, there is no reasonable fit with the data, be it Bayesian or frequentist.

(ii) Even within the framework of the SM, the color-suppressed tree amplitude, C, may be significantly larger than the naive prediction. If we extend the allowed region for C, keeping $|C|/|T| \leq 0.5$, we are still in the SM-like region, but the fit is considerably improved; in fact, one obtains a perfectly acceptable fit, and the fitted value of $\Delta A_{\rm CP}$ is within 2σ of the global average when the color-suppressed tree amplitude is allowed to vary in the above mentioned range. We have checked the allowed region with several fits, neglecting and including suppressed contributions, and playing with the relative importance of the electroweak penguin WCs. Everything gives the same result; the posterior distribution is almost identical, and the suppressed amplitudes are hardly constrained.

Thus, the first conclusion is that there is no immediate need to go beyond the SM, although a more precise estimate of various amplitudes is welcome. There is now a tension of about 2σ between the global average and the best-fit value of Δ_{CP}; with more precise data this tension can grow and that will be a serious indication for beyond-SM dynamics.

There is a second conclusion, too. For the Double-κ fit, the parameter space shows another best-fit region, which, in fact, contains the global maximum-likelihood estimate. However, the region is far from what is allowed by the

SM. For this region, NP is definitely indicated. Thus, we have found that both the observables, namely, ΔA_{CP} and Δ_4, can differentiate between these two high-probability regions of parameter space, or, in other words, act as smoking guns for new physics. We, therefore, urge our experimental colleagues to measure this quantity as precisely as possible.

ACKNOWLEDGMENTS

The authors acknowledge the Science and Engineering Research Board, Government of India, for the Grants No. CRG/2019/000362 (A. K. and S. R.), No. MTR/2019/000066 and No. DIA/2018/000003(A. K.).

APPENDIX: BAYESIAN TERMINOLOGY

For a point or interval estimation of a parameter θ in a model M based on data y, Bayesian inference is based off the Bayes' Theorem,

$$p(\vec{\theta}|y) = \frac{p(y|\vec{\theta})p(\vec{\theta})}{p(y)} \propto p(y|\vec{\theta})p(\vec{\theta}), \tag{A1}$$

where

(1) $p(\vec{\theta})$ is the prior probability density (in short, *prior*) for the parameter-vector $\vec{\theta}$, encapsulating all of our initial knowledge about the parameters. In this work, the priors for the free parameters are set as uniform distributions of a very large range, whereas the theoretical inputs are incorporated as multidimensional Gaussian distributions.

(2) $p(y|\vec{\theta})$ is the 'likelihood function' (in short, *likelihood*). It quantifies the likelihood that the observed data would have been observed as a function of $\vec{\theta}$ (but it is not a probability density for $\vec{\theta}$).

(3) $p(y)$ is the evidence, defined as $p(y) = \int p(y|\vec{\theta})p(\vec{\theta})d\vec{\theta}$ and is just a constant for our purpose, i.e., parameter estimation.

(4) $p(\vec{\theta}|y)$ is the coveted posterior (or 'inverse', in old usage) probability distribution (in short, *posterior*) of $\vec{\theta}$, given the data y. We generate samples from this distribution (actually the unnormalized one, ignoring the generally intractable 'evidence') by running an MCMC process.

(5) For estimating any single parameter θ_j among n such parameters, we need to find the one-dimensional (1D) marginal distribution of that parameter by integrating the full posterior over all other parameters; $p(\theta_j|y) = \int p(y|\vec{\theta})d\theta_1 \ldots d\theta_{j-1}d\theta_{j+1}\ldots d\theta_n$. In practice, once the MCMC sample is generated, marginalizing is as trivial as neglecting all other parameter values from the sample. Similarly, higher-dimensional marginal posteriors can also be generated. Such 2D marginal posteriors are used to depict the parameter spaces in most places in this work.

Credible Intervals (CIs): In Bayesian parlance, the interval within which the appearance of an unobserved parameter value has a particular probability, is called a credible interval (credible region, for multivariate cases).

As we obtain a probability distribution (posterior) after a Bayesian analysis, point (central tendency) or interval (dispersion) estimation is not unique and quite problematic. The best Bayesian analog of the MLE is the maximum *a posteriori* probability (MAP) estimate, which is (a) really ambiguous for multimodal distributions (as in the case of the *'Real κ Global Order-2'* fit), (b) generally uncharacteristic of the majority of the posterior, and (c) is not invariant under re-parametrization. We have thus only mentioned medians as point estimates of parameters, only for the unimodal 'local' fits. Furthermore, the credible intervals (CIs) around these estimates, in addition to implying completely different conceptual things from confidence intervals (their frequentist analogs), depict different regions with different probability content, in general.

This is why we refrain from using the point estimates for calculating our numerical predictions, and instead use the whole posterior samples to do that.

[1] A. J. Buras, R. Fleischer, S. Recksiegel, and F. Schwab, The $B \to \pi K$ puzzle and its relation to rare B and K decays, Eur. Phys. J. C **32**, 45 (2003).

[2] A. J. Buras, R. Fleischer, S. Recksiegel, and F. Schwab, $B \to \pi\pi$, New Physics in $B \to \pi K$ and Implications for Rare K and B Decays, Phys. Rev. Lett. **92**, 101804 (2004).

[3] A. J. Buras, R. Fleischer, S. Recksiegel, and F. Schwab, Anatomy of prominent B and K decays and signatures of CP violating new physics in the electroweak penguin sector, Nucl. Phys. **B697**, 133 (2004).

[4] S. Baek, P. Hamel, D. London, A. Datta, and D. A. Suprun, The $B \to \pi K$ puzzle and new physics, Phys. Rev. D **71**, 057502 (2005).

[5] B. Aubert *et al.* (*BABAR* Collaboration), Improved measurements of the branching fractions for $B^0 \to \pi^+\pi^-$ and $B^0 \to K^+\pi^-$, and a search for $B^0 \to K^+K^-$, Phys. Rev. D **75**, 012008 (2007).

[6] B. Aubert *et al.* (*BABAR* Collaboration), Observation of $B^+ \to \bar{K}^0 K^+$ and $B^0 \to K^0 \bar{K}^0$, Phys. Rev. Lett. **97**, 171805 (2006).

[7] B. Aubert *et al.* (*BABAR* Collaboration), Study of $B^0 \to \pi^0\pi^0$, $B^\pm \to \pi^\pm\pi^0$, and $B^\pm \to K^\pm\pi^0$ decays, and isospin analysis of $B \to \pi\pi$ decays, Phys. Rev. D **76**, 091102 (2007).

[8] B. Aubert *et al.* (*BABAR* Collaboration), Measurement of time dependent *CP* asymmetry parameters in B^0 meson decays to ωK^0_S, $\eta' K^0$, and $\pi^0 K^0_S$, Phys. Rev. D **79**, 052003 (2009).

[9] J. P. Lees *et al.* (*BABAR* Collaboration), Measurement of *CP* asymmetries and branching fractions in charmless two-body *B*-meson decays to pions and kaons, Phys. Rev. D **87**, 052009 (2013).

[10] M. Fujikawa *et al.* (Belle Collaboration), Measurement of *CP* asymmetries in $B_0 \to K_0\pi_0$ decays, Phys. Rev. D **81**, 011101 (2010).

[11] Y. T. Duh *et al.* (Belle Collaboration), Measurements of branching fractions and direct *CP* asymmetries for $B \to K\pi$, $B \to \pi\pi$ and $B \to KK$ decays, Phys. Rev. D **87**, 031103 (2013).

[12] R. Aaij *et al.* (LHCb Collaboration), Branching fraction and *CP* asymmetry of the decays $B^+ \to K^0_S\pi^+$ and $B^+ \to K^0_S K^+$, Phys. Lett. B **726**, 646 (2013).

[13] R. Aaij *et al.* (LHCb Collaboration), Measurement of *CP* asymmetries in two-body $B^0_{(s)}$-meson decays to charged pions and kaons, Phys. Rev. D **98**, 032004 (2018).

[14] R. Aaij *et al.* (LHCb Collaboration), Observation of *CP* violation in two-body $B^0_{(s)}$-meson decays to charged pions and kaons, J. High Energy Phys. 03 (2021) 075.

[15] F. Abudinén *et al.* (Belle-II Collaboration), Measurements of branching fractions and direct *CP* asymmetries in $B^0 \to K^+\pi^-$, $B^+ \to K^0_S\pi^+$ and $B^0 \to \pi^+\pi^-$ using 2019 and 2020 data, arXiv:2106.03766.

[16] F. Abudinén *et al.* (Belle-II Collaboration), Measurements of branching fractions and direct *CP*-violating asymmetries in $B^+ \to K^+\pi^0$ and $\pi^+\pi^0$ decays using 2019 and 2020 Belle II data, arXiv:2105.04111.

[17] F. Abudinén *et al.* (Belle II Collaboration), First search for direct *CP*-violating asymmetry in $B^0 \to K^0\pi^0$ decays at Belle II, arXiv:2104.14871.

[18] R. Aaij *et al.* (LHCb Collaboration), Measurement of *CP* Violation in the Decay $B^+ \to K^+\pi^0$, Phys. Rev. Lett. **126**, 091802 (2021).

[19] M. Gronau and J. L. Rosner, Combining *CP* asymmetries in $B \to K\pi$ decays, Phys. Rev. D **59**, 113002 (1999).

[20] M. Gronau, O. F. Hernandez, D. London, and J. L. Rosner, Decays of *B* mesons to two light pseudoscalars, Phys. Rev. D **50**, 4529 (1994).

[21] M. Gronau, O. F. Hernandez, D. London, and J. L. Rosner, Electroweak penguins and two-body *B* decays, Phys. Rev. D **52**, 6374 (1995).

[22] M. Gronau, O. F. Hernandez, D. London, and J. L. Rosner, Broken SU(3) symmetry in two-body *B* decays, Phys. Rev. D **52**, 6356 (1995).

[23] M. Neubert, Rescattering effects, isospin relations and electroweak penguins in $B \to \pi K$ decays, Phys. Lett. B **424**, 152 (1998).

[24] D. Atwood and A. Soni, The possibility of large direct *CP* violation in $B \to K\pi$—like modes due to long distance rescattering effects and implications for the angle γ, Phys. Rev. D **58**, 036005 (1998).

[25] A. J. Buras, R. Fleischer, and T. Mannel, Penguin topologies, rescattering effects and penguin hunting with $B_{u,d} \to K\bar{K}$ and $B^\pm \to \pi^\pm K$, Nucl. Phys. **B533**, 3 (1998).

[26] A. J. Buras and R. Fleischer, Constraints on the CKM angle γ and strong phases from $B \to \pi K$ decays, Eur. Phys. J. C **16**, 97 (2000).

[27] A. F. Falk, A. L. Kagan, Y. Nir, and A. A. Petrov, Final state interactions and new physics in $B \to \pi K$ decays, Phys. Rev. D **57**, 4290 (1998).

[28] A. J. Buras and L. Silvestrini, Nonleptonic two-body *B* decays beyond factorization, Nucl. Phys. **B569**, 3 (2000).

[29] M. Beneke, G. Buchalla, M. Neubert, and C. T. Sachrajda, QCD factorization for exclusive, nonleptonic *B* meson decays: General arguments and the case of heavy light final states, Nucl. Phys. **B591**, 313 (2000).

[30] C. W. Bauer and D. Pirjol, Graphical amplitudes from SCET, Phys. Lett. B **604**, 183 (2004).

[31] C. W. Bauer, D. Pirjol, I. Z. Rothstein, and I. W. Stewart, $B \to M_1 M_2$: Factorization, charming penguins, strong phases, and polarization, Phys. Rev. D **70**, 054015 (2004).

[32] C. W. Bauer, I. Z. Rothstein, and I. W. Stewart, SCET analysis of $B \to K\pi$, $B \to K\bar{K}$, and $B \to \pi\pi$ decays, Phys. Rev. D **74**, 034010 (2006).

[33] M. Beneke, G. Buchalla, M. Neubert, and C. T. Sachrajda, QCD factorization in $B \to \pi K$, $\pi\pi$ decays and extraction of Wolfenstein parameters, Nucl. Phys. **B606**, 245 (2001).

[34] K. Huitu and S. Khalil, New physics contribution to $B \to K\pi$ decays in SCET, Phys. Rev. D **81**, 095008 (2010).

[35] S. Nandi and A. Kundu, Large electroweak penguins in $B \to \pi\pi$ and $B \to \pi K$: Implication for new physics, arXiv:hep-ph/0407061.

[36] D. Chang, C. S. Chen, H. Hatanaka, and C. S. Kim, Generalized study with isospin-phased topological approach on the $B \to K\pi$ puzzle, arXiv:hep-ph/0510328.

[37] S. Baek, New physics in $B \to \pi\pi$ and $B \to \pi K$ decays, J. High Energy Phys. 07 (2006) 025.

[38] S. Baek and D. London, Is there still a $B \to \pi K$ puzzle?, Phys. Lett. B **653**, 249 (2007).

[39] C. S. Kim, S. Oh, and Y. W. Yoon, Analytic resolution of puzzle in $B \to K\pi$ decays, Phys. Lett. B **665**, 231 (2008).

[40] T. Feldmann, M. Jung, and T. Mannel, Is there a non-standard-model contribution in non-leptonic $b \to s$ decays?, J. High Energy Phys. 08 (2008) 066.

[41] M. Ciuchini, E. Franco, G. Martinelli, M. Pierini, and L. Silvestrini, Searching for new physics with $B \to K\pi$ decays, Phys. Lett. B **674**, 197 (2009).

[42] S. Baek, C.-W. Chiang, and D. London, The $B \to \pi K$ puzzle: 2009 update, Phys. Lett. B **675**, 59 (2009).

[43] S. Baek, C.-W. Chiang, M. Gronau, D. London, and J. L. Rosner, Diagnostic for new physics in $B \to \pi K$ decays, Phys. Lett. B **678**, 97 (2009).

[44] N. B. Beaudry, A. Datta, D. London, A. Rashed, and J.-S. Roux, The $B \to \pi K$ puzzle revisited, J. High Energy Phys. 01 (2018) 074.

[45] R. Fleischer, R. Jaarsma, and K. K. Vos, Towards new frontiers with $B \to \pi K$ decays, Phys. Lett. B **785**, 525 (2018).

[46] R. Fleischer, R. Jaarsma, E. Malami, and K. K. Vos, Exploring $B \to \pi\pi, \pi K$ decays at the high-precision frontier, Eur. Phys. J. C **78**, 943 (2018).

[47] M. Imbeault, Relative sizes of diagrams in $B \to \pi\pi$, πK decays, arXiv:hep-ph/0505254.

[48] Y. Y. Keum, H.-N. Li, and A. I. Sanda, Penguin enhancement and $B \to K\pi$ decays in perturbative QCD, Phys. Rev. D **63**, 054008 (2001).

[49] M. Beneke and M. Neubert, QCD factorization for $B \to PP$ and $B \to PV$ decays, Nucl. Phys. **B675**, 333 (2003).

[50] Q. Chang, X.-Q. Li, and Y.-D. Yang, Revisiting $B \to \pi K$, πK^* and ρK decays: Direct CP violation and implication for new physics, J. High Energy Phys. 09 (2008) 038.

[51] H.-Y. Cheng and C.-K. Chua, Resolving $B - CP$ puzzles in QCD factorization, Phys. Rev. D **80**, 074031 (2009).

[52] H.-n. Li and S. Mishima, Possible resolution of the $B \to \pi\pi$, πK puzzles, Phys. Rev. D **83**, 034023 (2011).

[53] H.-n. Li and S. Mishima, Glauber gluons in spectator amplitudes for $B \to \pi M$ decays, Phys. Rev. D **90**, 074018 (2014).

[54] X. Liu, H.-N. Li, and Z.-J. Xiao, Resolving the $B \to K\pi$ puzzle by Glauber-gluon effects, Phys. Rev. D **93**, 014024 (2016).

[55] A. Datta and D. London, Measuring new physics parameters in B penguin decays, Phys. Lett. B **595**, 453 (2004).

[56] M. Imbeault, D. London, C. Sharma, N. Sinha, and R. Sinha, Patterns of new physics in B decays, Phys. Lett. B **653**, 254 (2007).

[57] L. Hofer, D. Scherer, and L. Vernazza, $B_s \to \phi\rho^0$ and $B_s \to \phi\pi^0$ as a handle on isospin-violating new physics, J. High Energy Phys. 02 (2011) 080.

[58] A. Crivellin, C. Gross, S. Pokorski, and L. Vernazza, Correlating ϵ'/ϵ to hadronic B decays via $U(2)^3$ flavour symmetry, Phys. Rev. D **101**, 015022 (2020).

[59] L. Calibbi, A. Crivellin, F. Kirk, C. A. Manzari, and L. Vernazza, Z' models with less-minimal flavour violation, Phys. Rev. D **101**, 095003 (2020).

[60] B. Bhattacharya, A. Datta, D. Marfatia, S. Nandi, and J. Waite, Axion-like particles resolve the $B \to \pi K$ and g-2 anomalies, Phys. Rev. D **104**, 051701 (2021).

[61] A. Datta, D. Sachdeva, and J. Waite, Unified explanation of $b \to s\mu^+\mu^-$ anomalies, neutrino masses, and $B \to \pi K$ puzzle, Phys. Rev. D **100**, 055015 (2019).

[62] Y. Nir and H. R. Quinn, Measuring CKM Parameters with CP Asymmetry and Isospin Analysis in $B \to \pi K$, Phys. Rev. Lett. **67**, 541 (1991).

[63] H. J. Lipkin, Y. Nir, H. R. Quinn, and A. Snyder, Penguin trapping with isospin analysis and CP asymmetries in B decays, Phys. Rev. D **44**, 1454 (1991).

[64] M. Neubert, Model independent analysis of $B \to \pi K$ decays and bounds on the weak phase gamma, J. High Energy Phys. 02 (1999) 014.

[65] R. Fleischer and T. Mannel, Constraining the CKM angle γ and penguin contributions through combined $B \to \pi K$ branching ratios, Phys. Rev. D **57**, 2752 (1998).

[66] M. Gronau and J. L. Rosner, Weak phase γ from ratio of $B \to K\pi$ rates, Phys. Rev. D **57**, 6843 (1998).

[67] M. Neubert and J. L. Rosner, New bound on γ from $B^\pm \to \pi K$ decays, Phys. Lett. B **441**, 403 (1998).

[68] M. Neubert and J. L. Rosner, Determination of the Weak Phase γ from Rate Measurements in $B^\pm \to \pi K$, $\pi\pi$ Decays, Phys. Rev. Lett. **81**, 5076 (1998).

[69] M. Gronau and J. L. Rosner, Rate and CP-asymmetry sum rules in $B \to K\pi$, Phys. Rev. D **74**, 057503 (2006).

[70] L.-L. Chau, H.-Y. Cheng, W. K. Sze, H. Yao, and B. Tseng, Charmless nonleptonic rare decays of B mesons, Phys. Rev. D **43**, 2176 (1991); **58**, 019902(E) (1998).

[71] M. Gronau, A precise sum rule among four $B \to K\pi CP$ asymmetries, Phys. Lett. B **627**, 82 (2005).

[72] G. Buchalla, A. J. Buras, and M. E. Lautenbacher, Weak decays beyond leading logarithms, Rev. Mod. Phys. **68**, 1125 (1996).

[73] M. Gronau, D. Pirjol, and T.-M. Yan, Model independent electroweak penguins in B decays to two pseudoscalars, Phys. Rev. D **60**, 034021 (1999); **69**, 119901(E) (2004).

[74] P. A. Zyla *et al.* (Particle Data Group Collaboration), Review of particle physics, Prog. Theor. Exp. Phys. **2020**, 083C01 (2020).

[75] A. Bornheim *et al.* (CLEO Collaboration), Measurements of charmless hadronic two body B meson decays and the ratio $\mathrm{B}(B \to DK)/\mathrm{B}(B \to D\pi)$, Phys. Rev. D **68**, 052002 (2003); **75**, 119907(E) (2007).

[76] T. A. Aaltonen *et al.* (CDF Collaboration), Measurements of Direct CP -Violating Asymmetries in Charmless Decays of Bottom Baryons, Phys. Rev. Lett. **113**, 242001 (2014).

[77] T. H. F. A. G. (HFLAV), Results on time-dependent CP1 violation, and measurements related to the angles of the unitarity triangle: Summer 2018.

[78] Y. S. Amhis *et al.* (HFLAV Collaboration), Averages of b-hadron, c-hadron, and τ-lepton properties as of 2018, Eur. Phys. J. C **81**, 226 (2021).

[79] N. Metropolis, A. W. Rosenbluth, M. N. Rosenbluth, A. H. Teller, and E. Teller, Equation of state calculations by fast computing machines, J. Chem. Phys. **21**, 1087 (1953).

[80] A. E. Raftery and S. Lewis, *How many iterations in the gibbs sampler?*, edited by J. M. Bernardo, J. O. Berger, A. P. Dawid, and A. F. M. Smith, Bayesian Statistics 4 (Oxford University Press, 1992), p. 763.

[81] C.-W. Chiang and Y.-F. Zhou, Flavor SU(3) analysis of charmless B meson decays to two pseudoscalar mesons, J. High Energy Phys. 12 (2006) 027.